Paper:

Helbig, M., Chasmer, L., Kljun, N., Quinton, W., Treat, C. & Sonnentag, O. (2016). The positive net radiative greenhouse gas forcing of increasing methane emissions from a thawing boreal forest-wetland landscape. *Global Change Biology*

http://dx.doi.org/10.1111/gcb.13520

Received Date : 11-Aug-2016

Accepted Date : 20-Sep-2016

Article type : Primary Research Articles

The positive net radiative greenhouse gas forcing of increasing methane emissions from a thawing boreal forest-wetland landscape

Helbig M[1]*, Chasmer L[2], Kljun N[3], Quinton W L[4], Treat C C[5,6], Sonnentag O[1]

[1]*Université de Montréal & Centre d'études nordiques*

Département de géographie

520 Chemin de la Côte Sainte-Catherine

Montréal, QC H2V 2B8, Canada

[2]*University of Lethbridge, Department of Geography, Lethbridge AB T1K 3M4, Canada*

[3]*Swansea University, Department of Geography, Singleton Park, Swansea SA28PP, UK*

[4]*Wilfrid Laurier University, Cold Regions Research Centre, Waterloo ON N2L 3C5, Canada*

[5]*University of Alaska Fairbanks, Water and Environmental Research Center, Fairbanks AK 99775, USA*

[6]*U.S. Geological Survey, Menlo Park CA 94025, USA*

This article has been accepted for publication and undergone full peer review but has not been through the copyediting, typesetting, pagination and proofreading process, which may lead to differences between this version and the Version of Record. Please cite this article as doi: 10.1111/gcb.13520

*corresponding author:

tel. 438-826-1985

email: manuel.helbig@umontreal.ca

Running head: Thaw-induced increase in methane emissions

Keywords: Climate change, Eddy covariance, Methane, Boreal forest, Wetland, Radiative forcing, Carbon dioxide

Submitted to: *Global Change Biology*

Primary Research Article

Abstract

At the southern margin of permafrost in North America, climate change causes widespread permafrost thaw. Here, thawing permafrost in forested peat plateaus ("forest") leads to expansion of permafrost-free wetlands ("wetland") in boreal lowlands. Expanding wetland area with saturated and warmer organic soils is expected to increase landscape methane (CH_4) emissions. Here, we quantify the thaw-induced increase in CH_4 emissions for a boreal forest-wetland landscape in the southern Taiga Plains, Canada, and evaluate its impact on net radiative forcing relative to potential long-term net carbon dioxide (CO_2) exchange. Using nested wetland and landscape eddy covariance net CH_4 flux measurements in combination with flux footprint modeling, we find that landscape CH_4 emissions increase with increasing wetland-to-forest ratio. Landscape CH_4 emissions are most sensitive to this ratio during peak emission periods, when wetland soils are up to 10 °C warmer than forest soils. The cumulative growing season (May - October) wetland CH_4 emissions of ~13 g CH_4 m^{-2} is the dominating contribution to the landscape CH_4 emissions of ~7 g CH_4 m^{-2}. In contrast, forest contributions to landscape CH_4 emissions appear to be negligible. The rapid wetland expansion of 0.26±0.05 % yr^{-1} in this region causes an estimated growing season increase of 0.034±0.007 g CH_4 m^{-2} yr^{-1} in landscape CH_4 emissions. A long-term net CO_2 uptake of > 200 g CO_2 m^{-2} yr^{-1} is required to offset the positive radiative forcing of increasing CH_4 emissions until the end of the 21st century as indicated by an atmospheric CH_4 and CO_2 concentration model. However, long-term apparent carbon accumulation rates in similar boreal forest-wetland landscapes and landscape eddy covariance net CO_2 flux measurements suggest a long-term net CO_2 uptake between 49 and 157 g CO_2 m^{-2} yr^{-1}. Thus, thaw-induced CH_4 emission increases likely exert a positive net radiative greenhouse gas forcing through the 21st century.

Introduction

Current global climate change is mainly attributed to rapidly rising atmospheric concentrations of two greenhouse gases, carbon dioxide (CO_2) and methane (CH_4) (Myhre *et al.*, 2013). The climate system impacts of changing greenhouse gas concentrations and other forcings is commonly expressed by their influence on the top-of-atmosphere net energy flux, referred to as radiative forcing (W m^{-2}; Myhre *et al.*, 2013). From 1750 to 2011, the radiative forcing resulting from increasing atmospheric CH_4 concentrations accounted for about a quarter of the radiative forcing from rising CO_2 concentrations. The recent increase in radiative forcing from CH_4 emissions has been mainly attributed to increasing anthropogenic CH_4 emissions (Myhre *et al.*, 2013; Nisbet *et al.*, 2014). Wetlands represent the largest natural CH_4 source to the atmosphere contributing about a third (177-284 Tg CH_4 yr^{-1}) of the total global CH_4 emissions (500 to 600 Tg CH_4 yr^{-1}; Dlugokencky *et al.*, 2011; Bridgham *et al.*, 2013; Melton *et al.*, 2013; Kirschke *et al.*, 2013). Inter-annual variations in wetland CH_4 emissions contribute 70 % of the variability in total global CH_4 emissions (Bousquet *et al.*, 2006). Despite the importance of wetlands for the global atmospheric CH_4 budget, estimates of wetland CH_4 emissions are still poorly constrained (Kirschke *et al.*, 2013).

Many boreal wetlands have slowly accumulated thick peat layers since the last ice age (Treat *et al.*, 2016), storing now about 436 Pg of soil organic carbon (C) as peat (i.e., north of 45°N; Loisel *et al.*, 2014). Despite their large C stocks and prevailing anoxic conditions, these boreal peatlands contribute relatively little (~20%) to global wetland CH_4 emissions (Bridgham *et al.*, 2013) due to the temperature-limitation in microbial CH_4 production (Dunfield *et al.*, 1993; Frolking *et al.*, 2011; Treat *et al.*, 2014). Thus, boreal peatlands sequester CO_2 from the atmosphere and, ultimately, re-emit a small proportion of the fixed C as CH_4 (Frolking *et al.*, 2011). About 278 Pg C is contained in peatlands of the northern circumpolar permafrost region (Tarnocai *et al.*, 2009). Increasingly warmer air temperatures, altered hydrology, and thawing of perennially frozen organic soils within this region, however, could result in enhanced microbial CH_4 production through warmer soils and higher water levels (e.g., Schuur *et al.*, 2015). Additionally, permafrost thaw in boreal peatlands often leads to shifts in vegetation communities toward more aquatic species (e.g., sedges; Camill, 1999). Increasing sedge density with deeper roots may enhance CH_4 production through the addition of easily decomposable root litter and root exudates (Prater *et al.*, 2007; Chanton *et al.*, 2008). Additionally, the presence of sedges may enhance plant-mediated CH_4 transport through their aerenchymous tissue. Methane oxidation above the water table is then minimized as CH_4 bypasses the otherwise diffusional CH_4 transport through the aerobic soil layers (Treat *et al.*, 2007; Olefeldt *et al.*, 2013). Ebullition, the transport of CH_4 with gas bubbles, also minimizes CH_4 oxidation and has been observed to increase with thawing permafrost and associated flooding of surface soils (Klapstein *et al.*, 2014). Better-constrained CH_4 emission estimates for boreal peatlands in the permafrost region and a better understanding of their environmental drivers are crucial for well-constrained projections of boreal peatland contributions to global net radiative forcing (Bousquet *et al.*, 2006; Dlugokencky *et al.*, 2009; Schuur *et al.*, 2015).

Permafrost at the southern margin of its distribution persists in disequilibrium with the current climate (e.g.; Camill & Clark, 1998). Here, increased energy input has resulted in extensive permafrost loss in boreal lowlands of North America where relatively dry forested permafrost peat plateaus ("forest") are replaced with wetter, treeless, permafrost-free collapse-scar bogs and fens ("wetland") resulting in highly fragmented landscapes (Quinton *et al.*, 2011; Baltzer *et al.*, 2014; Lara *et al.*, 2016; Helbig *et al.*, 2016a). Chamber-based studies in such heterogeneous boreal forest-wetland landscapes have identified wetlands as major CH_4 emission sources, while forests remain comparatively small net CH_4 sources or sinks (Moore *et al.*, 1994; Liblik *et al.*, 1997; Turetsky *et al.*, 2002; Bubier *et al.*, 2005; Johnston *et al.*, 2014). Current thaw-induced wetland expansion and associated forest loss in northwestern Canada (e.g., Baltzer *et al.*, 2014) in combination with increasing air and soil temperatures are therefore expected to further enhance regional CH_4 emissions over the next few decades (Liblik *et al.*, 1997; Moore *et al.*, 1998; Johnston *et al.*, 2014).

Here, we first integrate nested eddy covariance ecosystem and landscape net CH_4 flux (F_{CH4}; nmol m^{-2} s^{-1}) measurements (Desai *et al.*, 2015) with flux footprint modeling and remotely sensed land cover data (e.g., Chasmer *et al.*, 2008; Kljun *et al.*, 2015) to better understand the spatial and temporal variability of F_{CH4} across a heterogeneous and rapidly thawing boreal forest-wetland landscape in the southern Taiga Plains ecozone of northwestern Canada. Next, we quantify the net radiative greenhouse gas (CH_4 and CO_2) forcing of thaw-induced F_{CH4} changes of the boreal forest-wetland landscape using a dynamic atmospheric CH_4 and CO_2 concentration model (Frolking *et al.*, 2006). The objectives of our study are to

(1) describe how F_{CH4} of a boreal forest-wetland landscape vary spatially with wetland extent and temporally with soil temperature and water table depth,

(2) quantify the impact of thaw-induced wetland expansion on landscape F_{CH4}, and

(3) assess the net radiative forcing of thaw-induced landscape F_{CH4} changes and concurrent net CO_2 uptake rates.

Materials and Methods

Study site

The study site, the Scotty Creek watershed, NT (61°18' N; 121°18' W), is located in the sporadic permafrost zone (>10 % - 50 % in areal extent) of the southern Taiga Plains ecozone of northwestern Canada (Quinton *et al.*, 2011). The southern part of Scotty Creek is dominated by forested permafrost peat plateaus (*Picea mariana*, ericaceous shrubs [mainly *Rhododendron groenlandicum*], lichens [*Cladonia* spp.] and bryophythes [*Sphagnum fuscum* and *S.*

capillifolium]) and treeless, permafrost-free collapse-scar bogs (ericaceous shrubs [*Chamaedaphne calyculata*, *Andromeda polifolia*, *Vaccinium oxycoccos*], bryophytes [*Sphagnum balticum* and *S. magellanicum*], pod grass [*Scheuchzeria palustris*]) (Garon-Labrecque *et al.*, 2015) with an organic layer thickness of >3 m and a mean total organic carbon content of 167±11 kg C m^{-2} (n = 3; N. Pelletier, unpublished results). More detailed descriptions of the study site can be found in Quinton *et al.* (2011), Baltzer *et al.* (2014), and Garon-Labrecque *et al.* (2015).

Eddy covariance measurements, flux data processing, and ancillary measurements

Between May 2013 and May 2016, F_{CH4} of the boreal forest-wetland landscape (F_{CH4_LAND}; nmol m^{-2} s^{-1}) was measured at a 15-m eddy covariance ("landscape") tower. Molar densities of CH_4 were measured with an open-path CH_4 analyzer (LI-7700, LI-COR Biosciences, Lincoln, NE) and the 3-D wind velocities with a sonic anemometer (CSAT3A, Campbell Scientific Inc., Logan, UT). Net water vapor (H_2O) and CO_2 fluxes were measured using an open-path CO_2/H_2O infrared gas analyzer (EC150, Campbell Scientific Inc., Logan, UT), except for the period March to June 2015 when an enclosed-path CO_2/H_2O infrared gas analyzer (LI-7200, LI-COR Biosciences) was used (see Helbig *et al.*, 2016b). The horizontal distance between the LI-7700 and the CSAT3A was 0.3 m and the vertical separation was 0.23 m.

At a nearby nested 2-m eddy covariance wetland (collapse-scar bog) tower, ecosystem F_{CH4} (F_{CH4_WET}; nmol m^{-2} s^{-1}) was measured between April 2014 and May 2016 using an instrumental setup identical to the landscape tower. The LI-7700 was installed at the same height as the CSAT3A, but was horizontally separated by 0.48 m. For both towers high-frequency 10-Hz turbulence data and CH_4, CO_2, and H_2O densities were recorded with CR3000 dataloggers (Campbell Scientific Inc.). At the end of the growing seasons, the LI-7700's were taken down (early November [2014 and 2015] and early September [2013]) and re-installed in late winter (between mid-March [2015 and 2016] and mid-April [2014]). The calibration of the LI-7700s was checked at the beginning and at the end of each growing season and twice during the growing season using the same zero (Ultra Zero Ambient Air, Praxair Canada Inc, Mississauga, ON, Canada) and 2.02-ppm CH_4 span gas (±0.1 ppm; Praxair Canada Inc.). No appreciable span or zero drift was observed. Forest (T_{s_FOR}, °C) and wetland soil temperatures (T_{s_WET}, °C) were measured near the eddy covariance towers at 32 cm below the moss surface using type T thermocouples (Omega Engineering, Stamford, CT, USA). Wetland water table depth (*WTD*, cm relative to the moss surface [center of wetland]) was measured in a perforated PVC tube using a vented pressure transducer (OTT PLS, Mellingen, Switzerland). A negative *WTD* indicates a water table below the moss surface. A more detailed description of the instrumental setup is given in Helbig *et al.* (2016c).

Turbulent gas fluxes were calculated using the EddyPro software (version 6.1.0, LI-COR Biosciences). Briefly, we used a double rotation for sonic anemometer tilt correction, removed spikes in the high-frequency time series (Vickers & Mahrt, 1997), corrected sonic temperature for humidity effects (Dijk *et al.*, 2004), and used block averaging for half-hour time series and a covariance maximization procedure to detect time lags. Analytical spectral corrections according to Moncrieff *et al.* (1997) and Moncrieff *et al.* (2004) were applied to account for low- and high-pass filtering effects, respectively. Temperature- and humidity-induced density fluctuations were compensated according to Webb *et al.* (1980) ["WPL term"]. To calculate F_{CH4}, corrections for spectroscopic effects were incorporated in the WPL term (McDermitt *et al.*, 2010). Half-hourly F_{CH4} were discarded when turbulence was not fully developed or non-stationary (Mauder & Foken, 2011), or when F_{CH4} were identified as outliers (Papale *et al.*, 2006). F_{CH4} was not used in the analyses when the CH_4 signal quality was low (indicated by a LI-7700 Relative Signal Strength Indicator [RSSI] <20 %) or when turbulence was weak (i.e., a friction velocity threshold of 0.17 m s^{-1} [95 % confidence interval: 0.12 – 0.25 m s^{-1}] as determined according to Papale *et al.* (2006)).

Flux footprints for both towers were modeled according to Kljun *et al.* (2015) and coupled to a land cover classification map (Chasmer *et al.*, 2014) to derive the relative contributions from each land cover type to half-hourly flux measurements. The landscape flux footprints consisted mainly of forests and wetlands. In contrast, the wetland flux footprints mainly originated from the wetland just north of the landscape tower and were entirely located within the its long-term flux footprint (see Helbig *et al.*, 2016c). Landscape F_{CH4} were excluded from the analyses when contributions from a nearby lake exceeded 5 % and F_{CH4_WET} were excluded when wetland contributions were less than 95 %.

To obtain cumulative F_{CH4} (ΣF_{CH4}, g CH_4 m^{-2}), we gap-filled F_{CH4_LAND} and F_{CH4_WET} using the 'marginal distribution sampling' method (Reichstein *et al.*, 2005), an extended look-up table method taking into account temporal autocorrelation. For the look-up tables, we used T_{s_WET}, *WTD*, and wind speed. We chose T_{s_WET} at 32 cm because maximum CH_4 production in peatlands was found to peak at about 20 cm below the water table (e.g., Kettunen *et al.*, 1999), corresponding to a depth of about 30 cm in the studied wetland (median $WTD \approx$ -10 cm). Look-up table gap-filling methods yield reliable annual ΣF_{CH4} estimates with an uncertainty of about ±10 % (Hommeltenberg *et al.*, 2014). Growing season landscape ΣF_{CH4} (ΣF_{CH4_LAND}; g CH_4 m^{-2} s^{-1}) and wetland ΣF_{CH4} (ΣF_{CH4_WET}; g CH_4 m^{-2} s^{-1}; defined for the snow-free period from May to October) were obtained by combining F_{CH4_LAND} and F_{CH4_WET} between May to August 2014 and September to October 2015 due to large gaps in F_{CH4_WET} in both years (Fig. 1). After quality control, gaps in F_{CH4_LAND} and F_{CH4_WET} totaled 64 % and 58 %, respectively. The uncertainty in ΣF_{CH4_LAND} and ΣF_{CH4_WET} was estimated as a combination of uncertainties introduced by the friction velocity threshold selection, by random errors in F_{CH4} measurements, and by uncertainties in gap-filled F_{CH4}. Briefly, ΣF_{CH4_LAND} and ΣF_{CH4_WET} was calculated for 100 friction velocity thresholds derived according to Papale *et al.* (2006). For each of the 100

F_{CH4_LAND} and F_{CH4_WET} time series, we randomly sampled 100 times from the error distributions of directly measured (random observation error) and gap-filled half hours (gap-filling error), resulting in 10,000 Σ F_{CH4_LAND} and ΣF_{CH4_WET} estimates. We used the standard deviation of F_{CH4} for similar meteorological conditions within ± 7-day windows, as derived from the gap-filling algorithm, to obtain half-hourly random observation and gap-filling error estimates (Moffat *et al.*, 2007; Lasslop *et al.*, 2008). Random observation errors were then scaled with the magnitude of gap-filled F_{CH4} and RSSI to obtain continuous time series of half-hourly random observation errors. We derived continuous time series of half-hourly gap-filling errors by scaling gap-filling errors with the magnitude of gap-filled F_{CH4} (Lasslop *et al.*, 2008). Then, 95 % confidence intervals were derived from the 10,000 ΣF_{CH4_LAND} and ΣF_{CH4_WET} estimates. By combining F_{CH4_LAND} and F_{CH4_WET} from 2014 (colder and drier than normal [1981 – 2010]) and 2015 (warmer and wetter), two years with differing meteorological conditions (Environment Canada, http://climate.weather.gc.ca/climate_data/daily_data_e.html?StationID=52780), we assume that growing season ΣF_{CH4_LAND} and ΣF_{CH4_WET} were approximately representative of their respective long-term growing season cumulative F_{CH4} sums.

Spatial and temporal controls and spectral decomposition of F_{CH4}

Methane production in anoxic soils increases with microbial activity and may be limited by, amongst others, temperature or substrate availability (Dunfield *et al.*, 1993). With the water table position close to the surface or with a minimized CH_4 oxidation potential due to plant-mediated CH_4 transport or ebullition, most of the produced CH_4 is emitted to the atmosphere (Sundh *et al.*, 1994; Bellisario *et al.*, 1999; Kettunen *et al.*, 1999; Moore *et al.*, 2011). In this case, temporal F_{CH4} variations are closely linked to CH_4 production rates, which are often controlled by soil temperature or vegetation productivity (e.g., Christensen *et al.*, 2003; Shannon & White, 1994). The strong seasonality in soil temperature and vegetation productivity results in a strong low-frequency component of F_{CH4} (e.g., weeks to months; Rinne *et al.*, 2007). In contrast, the spectral signature of the spatial F_{CH4} footprint heterogeneity is expected to correspond to higher frequency components (e.g., hours), related to rapid changes in footprint composition with instantaneous effects on F_{CH4} measurements. This spatial footprint variability has often been classified as part of the random error in eddy covariance flux measurements (Moncrieff *et al.*, 1996). Recent developments in flux footprint models and remote sensing open new opportunities to analyze the direct control of such footprint heterogeneity on eddy covariance fluxes (e.g., Chasmer *et al.*, 2008; Kljun *et al.*, 2015; Helbig *et al.*, 2016c).

To decompose F_{CH4_LAND} and F_{CH4_WET} into low- (F_{CH4_sf}, nmol m^{-2} s^{-1}) and high-frequency components (F_{CH4_hf}, nmol m^{-2} s^{-1}), we used a modification of Singular Spectrum Analysis (SSA; Schoellhamer (2001). This time series analysis technique accounts for missing data in time series (Schoellhamer, 2001) and enhances the signal-to-noise ratio (Mahecha *et al.*, 2007). The time series is decomposed into linearly superimposed frequency-specific sub-signals that can then be partially reconstructed by specifying individual frequencies. We calculated F_{CH4_sf} by selecting frequencies longer than one week (seasonal) and F_{CH4_hf} by selecting frequencies between two hours to seven days (sub-weekly). Frequencies smaller than two hours were not analyzed to reduce noise introduced by F_{CH4_LAND} and F_{CH4_WET} measurements during periods with low RSSI signal strength (Fig. S1). A detailed discussion of SSA for eddy covariance flux studies can be found in Mahecha *et al.* (2007).

The control of flux footprint composition (i.e., contributions from wetlands [FP_{WET}, %]) on F_{CH4_LAND} and of T_{s_WET} and *WTD* on F_{CH4_LAND} and F_{CH4_WET} were analyzed independently. Linear regressions between FP_{WET} and F_{CH4_LAND} were applied to three-day moving windows. By constraining linear regressions to a short time period, the seasonal evolution of spatial F_{CH4} heterogeneities in landscape flux footprints can be tracked. To assess the most important seasonal F_{CH4_LAND} and F_{CH4_WET} (i.e., F_{CH4_sf}) controls, we conducted a multiple linear regression applying a stepwise forward selection procedure (Legendre & Legendre, 2012) for the variables T_{s_WET}, *WTD*, and the interaction term between T_{s_WET} and *WTD*. For the regression, we used 10000 randomly selected subsets of 30 F_{CH4_sf} data points to minimize the effects of temporal autocorrelation.

Wetland flux footprints almost exclusively comprised wetland surfaces. In contrast, landscape flux footprints comprised varying contributions of wetland and forest surfaces, but forests never contributed more than 90 % to the flux footprints. Thus, we fitted Q_{10}-models to F_{CH4_LAND} and F_{CH4_WET} for classes of increasing forest contribution to flux footprints to scale F_{CH4} to a hypothetical forest-only landscape (F_{CH4_FOR}; nmol m^{-2} s^{-1}) and to assess its response to T_{s_WET}:

$$F_{CH4\_i} = F_{CH4\_base\_i}\, Q_{10\_i}^{[T_{s\_WET}-10]/10} \qquad (1)$$

where *i* stands for the *i*-th forest contribution class, F_{CH4_base} is the reference F_{CH4} at T_{s_WET} = 10 °C, and Q_{10} is an indicator of the temperature sensitivity of F_{CH4_i}. The Q_{10} models were fitted to F_{CH4} with <10 % forest footprint contributions (i.e., F_{CH4_WET}) and to four classes of increasing forest contribution to landscape flux footprints (i.e., F_{CH4_LAND}).

Net radiative greenhouse gas forcing

The net radiative greenhouse gas forcing (W m^{-2}) of persistent thaw-induced increases in CH_4 emissions and concurrent net CO_2 exchange was calculated using a dynamic model of atmospheric CH_4 and CO_2 pools (Frolking *et al.*, 2006; Neubauer & Megonigal, 2015). The time-dependent evolution of the atmospheric CH_4 concentration perturbation (r_{CH4}; g CH_4 m^{-2}) of an annual CH_4 emission (r_{0_CH4}; g CH_4 m^{-2} yr^{-1}) was computed as a simple exponential decay:

$$r_{CH4}\,(t) = r_{0\_CH4} \exp\left(\frac{-t}{\tau_{CH4}}\right) \qquad (2)$$

where the atmospheric lifetime of CH_4 (τ_{CH4}) is 12.4 years (Myhre *et al.*, 2013). The evolution of the atmospheric CO_2 concentration perturbation (r_{CO2}, g CO_2 m^{-2}) of annual CO_2 uptake (r_{0_CO2}; g CO_2 m^{-2} yr^{-1}) was modeled as the sum of exponentials for five atmospheric pools with lifetimes (τ_i) ranging from the "slowest" pool with 10^8 years to the "fastest" pool with 3.4 years accounting for the varying redistribution timescales of CO_2 within the ocean, the land biosphere, and the atmosphere. A fraction of r_{0_CO2} (α_i) is attributed to each atmospheric CO_2 pool (Joos *et al.*, 2013). Values for τ_i and α_i in:

$$r_{CO2}(t) = \sum_{i=0}^{4} \alpha_i \, r_{0\_CO2} \exp\left(\frac{-t}{\tau_i}\right) \quad (3)$$

are as in Frolking *et al.* (2006). Both models were run for 100-year time series of r_{0_CH4} and r_{0_CO2}. The radiative forcing (RF, W m^{-2}) of greenhouse gas i (CH_4 and CO_2) is then calculated as follows:

$$RF_i = f_i A_i \, r_i \quad (4)$$

where f_i for CH_4 [1.65, Myhre *et al.* (2013)] accounts for indirect CH_4 effects on ozone concentrations and stratospheric H_2O and is 1 for CO_2, A_i is the radiative efficiency ($1.27*10^{-13}$ W m^{-2} kg^{-1} for CH_4 and $1.7517*10^{-15}$ W m^{-2} kg^{-1} for CO_2), and r_i is the current time atmospheric concentration perturbation of the respective greenhouse gas due to all previous emissions/uptake since a reference year (see Frolking *et al.* (2006)).

To estimate the future landscape CH_4 emissions (r_{0_CH4} in eq. 3), we derived and applied a mean annual wetland expansion rate of 0.26±0.05 % yr^{-1} (±95 % confidence interval; $n = 7$) from historical wetland extent changes between 1977 and 2010 for seven areas of interest at Scotty Creek (Baltzer *et al.*, 2014), resulting in an increase in wetland extent from 39 % in 1977 to 65 % in 2077. We estimated the trajectory of annual growing season $\Sigma F_{CH4\_LAND\_i}$ (eq. 5; where i stands for the year between 1977 and 2077) by combining the temporal trajectory of wetland-to-forest ratios (wet_i) with ΣF_{CH4_WET} and ΣF_{CH4_FOR}:

$$\Sigma F_{CH4\_LAND\_i} = wet_i \;\; \Sigma F_{CH4\_WET} + (1 - wet_i) \;\; \Sigma F_{CH4\_FOR} \quad (5)$$

The prescribed $\Sigma F_{CH4\_LAND\_i}$ time series was then used as r_{0_CH4} in the atmospheric concentration model (eq. 2). Uncertainties in the prescribed $\Sigma F_{CH4\_LAND\_i}$ were estimated based on the 95 % confidence interval of annual wetland expansion rates. Simulations were run for 100 years (1977-2077), where 1977 is the reference year, the first year with an estimate of the spatial wetland extent at Scotty Creek (Baltzer *et al.*, 2014).

Long-term annual net CO_2 uptake in high-latitude peatland landscapes could potentially offset the positive radiative forcing of increasing landscape CH_4 emissions (Frolking *et al.*, 2006). To quantify radiative forcing related to net CO_2 exchange, we used long-term apparent rates of carbon accumulation (LARCA, g C m^{-2} yr^{-1}) from 63 boreal peatlands in the circumpolar permafrost zone in North America with a basal peat age of more than 1000 years, including (collapse-scar) bogs, (forested) peat plateaus, and fens (Treat *et al.*, 2016). Peatland LARCA itself is the result of long-term net CO_2 uptake, CH_4 emissions, and net aquatic C exports. We assume the latter to be negligible across the thawing boreal forest-wetland landscape (e.g., Moore, 2003; Olefeldt *et al.*, 2012; Neubauer, 2014). Carbon losses related to CH_4 emissions, approximated as the measured growing season ΣF_{CH4_LAND}, were added to LARCA to calculate the mean long-term net CO_2 uptake (r_{0_CO2} in the atmospheric concentration model; eq. 3). Using the mean long-term annual net CO_2 uptake rate accounts for interannual variability in net CO_2 uptake and disturbance losses of CO_2 (e.g., wildfires) and is therefore a more appropriate measure than, for example, annual net primary production, which does not account for decomposition after litterfall (Chapin *et al.*, 2006). Annual net ecosystem CO_2 exchange (NEE; g CO_2 m^{-2} yr^{-1}) accounts for such decomposition, but year-round NEE measurements are only available for a few boreal peatlands in the permafrost zone (e.g., Dunn *et al.*, 2007; Euskirchen *et al.*, 2014), do not account for CO_2 losses from fire disturbances (Chapin *et al.*, 2006), and uncertainties due to interannual NEE variability are usually large (Roulet *et al.*, 2007). To compare annual eddy covariance NEE to mean long-term net CO_2 uptake derived from LARCA, we also used annual landscape NEE at Scotty Creek for r_{0_CO2} (eq. 3). Our NEE estimate for Scotty Creek was based on one year of eddy covariance net CO_2 flux measurements at the landscape tower (Helbig *et al.*, 2016b).

Results

Spatial and temporal controls of F_{CH4}

To identify the most important drivers of F_{CH4_LAND} and F_{CH4_WET}, we analyzed the decomposed F_{CH4} signals at seasonal low-frequency (F_{CH4_sf}) and at sub-weekly high-frequency time scales (F_{CH4_hf}). At the wetland tower, F_{CH4_sf} contributed more to the total F_{CH4} variance (75 %) than at the landscape tower (40 %). In turn, F_{CH4_hf} contributed less to the total F_{CH4} variance at the wetland tower (12 %) compared to the landscape tower (39 %) (Fig. 1), highlighting the more pronounced heterogeneity of F_{CH4} in the landscape flux footprints.

Seasonal landscape and wetland F_{CH4_sf} were mainly controlled by $T_{s\_WET}^2$ (landscape r^2 = 0.82, $p < 0.001$ and wetland $r^2 = 0.84$, $p < 0.001$; Fig. S2). In July and August, T_{s_WET} peaked at ~16 °C and remained between 0 °C and 1 °C from December to April (Fig. S3). With a mean annual T_{s_WET} of 5.2±5.6 °C (±one standard deviation, for 2015) the wetland soil was substantially warmer than T_{s_FOR} (1.1±2.8 °C). The average *WTD* during the study period was -11±6 cm. The *WTD* peaked at +10 cm (i.e., above the moss surface) shortly after snowmelt (late April/early May in 2014 and 2015) and reached its lowest position below the surface with -20 cm in October 2014 (Fig. S3). The negative relationship between *WTD* and F_{CH4_sf} (i.e., larger F_{CH4_sf} with lower water table) explained 47 % of the variance in F_{CH4_sf} at the wetland tower (p = 0.002), but was not significant at the landscape tower (p = 0.12; Fig. S2). For a multiple linear regression with T_s^2, *WTD*, and their interaction term as explanatory variables of F_{CH4_sf}, only T_s^2 was significant at $\alpha = 0.05$ for both the landscape and the wetland tower.

In contrast to the wetland tower where F_{CH4_sf} dominated F_{CH4_WET}, F_{CH4_sf} and F_{CH4_hf} contributed equally to F_{CH4_LAND}. Sub-weekly F_{CH4_LAND} was mainly controlled by footprint composition when differences between T_{s_WET} and T_{s_FOR} were largest (Fig. 2). With decreasing T_{s_WET}-T_{s_FOR} differences, the sensitivity of F_{CH4_LAND} to FP_{WET} diminished. Thus, F_{CH4} contrasts between wetlands and forests were small in the winter with cold T_{s_WET} and T_{s_FOR} (~0 °C), and large in the summer when T_{s_WET} were up to 10 °C warmer than T_{s_FOR}.

The impact of changing wetland extents on landscape F_{CH4}

Eddy covariance measurements at the landscape tower and flux footprint modeling suggest that wetlands are the main CH_4 sources within the landscape (Fig. 2). Direct comparisons of F_{CH4_WET} to F_{CH4_LAND} support this result, as F_{CH4_LAND} were consistently smaller than F_{CH4_WET} (Fig. 3a). The two fluxes became more similar with increasing wetland contribution to landscape flux footprints (Tab. 1). When wetland contributions to F_{CH4_LAND} were large (70% - <90%), the F_{CH4_WET}-F_{CH4_LAND} regression slope was closest to unity with 0.74, and decreased to 0.34 with decreasing wetland contributions (10% - <30%), thus confirming the dominant contribution of wetlands to F_{CH4_LAND}.

The smallest F_{CH4_LAND} and the weakest response to T_{s_WET} were observed for the largest forest contributions (Fig. 3b). From the smallest to the largest forest contributions, F_{CH4_base} (see eq. 1) decreased consistently from 56 nmol m^{-2} s^{-1} to 20 nmol m^{-2} s^{-1}, while Q_{10} values changed only slightly (Tab. 2). To estimate the forest-only F_{CH4}, F_{CH4_FOR}, we derived a Q_{10}-model using a mean Q_{10} value (Tab. 2) and a scaled F_{CH4_base} estimate for forest-only contributions. To scale F_{CH4_base}, we conducted a regression of the median forest contributions of the five forest contribution classes (see Tab. 2) against F_{CH4_base} ($r^2 = 0.91$; $p = 0.01$; $n = 5$). The estimated F_{CH4_base} was not significantly different from zero with 2.6 nmol m^{-2} s^{-1} (95 % CI: -23 – 14 nmol m^{-2} s^{-1}) and modelled F_{CH4_FOR} remained <10 nmol m^{-2} s^{-1}, even at warm T_{s_WET} (Fig. 3b). Thus, F_{CH4_FOR} was insensitive to T_{s_WET} and negligible compared to F_{CH4_WET}.

Between April and October, monthly ΣF_{CH4_LAND} and ΣF_{CH4_WET} showed a distinct seasonal cycle (Fig. 4 a & b). Monthly ΣF_{CH4_LAND} increased from a minimum monthly ΣF_{CH4_LAND} of 0.2 g CH_4 m^{-2} in April 2015 & 2016 to a peak monthly ΣF_{CH4_LAND} of 2.2 g CH_4 m^{-2} in July & August 2015 before decreasing again to a minimum monthly ΣF_{CH4_LAND} of 0.5 g CH_4 m^{-2} in October 2014. Similarly, monthly ΣF_{CH4_WET} increased from a minimum of 0.5 g CH_4 m^{-2} in April 2016 to a peak monthly ΣF_{CH4_WET} of 3.9 g CH_4 m^{-2} in August 2015 before decreasing again to a minimum monthly ΣF_{CH4_WET} of 1.4 g CH_4 m^{-2} in October 2015. The largest relative interannual differences in monthly ΣF_{CH4_LAND} occurred in May and June 2014 with ΣF_{CH4_LAND} being about 50 % smaller than ΣF_{CH4_LAND} of the same months in 2015. During these months, T_{s_WET} was about 5 °C colder in 2014, while *WTD* was similar with differences of ±2 cm (Fig. 4 c).

Total growing season ΣF_{CH4_WET} was about twice (13.0 g CH_4 m^{-2}; 95 % CI: 12.8 – 13.1 g CH_4 m^{-2}) the ΣF_{CH4_LAND} (6.7 g CH_4 m^{-2}; 95 % CI: 6.6 – 6.8 g CH_4 m^{-2}; Fig. 5). The mean growing season forest contribution to landscape flux footprints was 46 % with wetlands contributing 52 % and the lake only 2 %. Wetland flux footprints always consisted of >95 % wetlands. To scale future growing season ΣF_{CH4_LAND} with changes in wetland-to-forest ratio (eq. 5), we assumed that growing season ΣF_{CH4_FOR} was negligible and independent of T_{s_WET} (Fig. 3b). Consequently, ΣF_{CH4_WET} was the dominant contribution to ΣF_{CH4_LAND} and a thaw-induced wetland expansion rate of 0.26±0.05 % yr^{-1} increases growing season ΣF_{CH4_LAND} by 0.034±0.007 g CH_4 m^{-2} yr^{-1} (~0.5 % of current ΣF_{CH4_LAND}).

Net radiative greenhouse gas forcing from a thawing boreal landscape

In the absence of long-term net CO_2 uptake, the increasing ΣF_{CH4_LAND} causes a steady rise in radiative forcing totaling 12.3±2.4 fW m^{-2} (fW = 10^{-15} W) after 100 years. An annual net CO_2 uptake of ~200 g CO_2 m^{-2} yr^{-1} would fully compensate for this positive radiative forcing (Fig. 6). However, long-term net CO_2 uptake rates between 49 g CO_2 m^{-2} yr^{-1} and 157 g CO_2 m^{-2} yr^{-1} of are characteristic for boreal peatlands similar to Scotty Creek (i.e., 90 % confidence interval of long-term net CO_2 uptake), with bogs and forested peat plateaus taking up less CO_2 than fens. The long-term annual net CO_2 uptake, required to compensate for the positive radiative CH_4 forcing is thus outside the range of both the observed annual NEE at Scotty Creek (-71 g CO_2 m^{-2} yr^{-1}, indicating a net CO_2 uptake) and the long-term net CO_2 uptake from similar boreal peatlands.

Discussion

Soil temperature and water table depth controls of temporal F_{CH4} variation

At the seasonal time scale, T_{s_WET} mainly controls F_{CH4_WET} and thus F_{CH4_LAND} (Fig. 1 & 2). In contrast, *WTD* exerts only a minor control over the seasonality of F_{CH4_WET} and F_{CH4_LAND}. At Scotty Creek, the wetland and forest water table positions are closest to the moss surface shortly after snowmelt, but decline as the growing season progresses with increasing evapotranspiration and lateral drainage (Connon *et al.*, 2015; Helbig *et al.*, 2016c; Fig. 4c). This water table drawdown occurs concurrently with T_{s_WET} getting warmer, inducing increasing F_{CH4_WET}, and consequently increasing F_{CH4_LAND}. Similarly, Bellisario *et al.* (1999) observed increasing CH_4 emissions with decreasing *WTD* for a boreal peatland with *WTD* > -15 cm. In a boreal minerotrophic fen with a similar *WTD* range as reported here, water table position only weakly affected F_{CH4} after accounting for soil temperature effects (Rinne *et al.*, 2007). At Scotty

Creek, wetland *WTD* was > -15 cm during 75 % of the growing season (May – October). The negative relationship between *WTD* and F_{CH4} may be reversed in drier years when the water table position falls below a certain threshold (e.g., below the zone of labile root exudate inputs; Treat *et al.*, 2007). Christensen *et al.* (2003) referred to the *WTD* control on F_{CH4} as an "on-off switch"; if the water table is within ~10 cm of the surface its effect on F_{CH4} is small compared to other environmental variables. Additionally, in some parts of the wetland, absolute water table fluctuations may be partly compensated by the vertical displacement of the peat surface itself (e.g., Bubier *et al.*, 1995; Sonnentag *et al.*, 2010). Methane emissions from wetlands with ground surface fluctuations are often less dependent on fluctuations in the absolute water table position (Hartley *et al.*, 2015).

Similar to the seasonal control of T_{s_WET} on F_{CH4}, T_{s_WET} may also control interannual ΣF_{CH4} variability. At Scotty Creek, smaller monthly ΣF_{CH4_LAND} in the early summer of 2014 appeared to be caused by ~5 °C colder wetland soils compared to 2015 (Fig. 4). This reduction in ΣF_{CH4_LAND} highlights the importance of T_{s_WET} for both seasonal and interannual F_{CH4} variability (Rask *et al.*, 2002; Christensen *et al.*, 2003).

Interannual ΣF_{CH4} variability may additionally be controlled by the average seasonal water table (Bubier *et al.*, 2005; Moore *et al.*, 2011). At Scotty Creek, *WTD* and T_s differences between forested peat plateaus and wetlands partly control the spatial variability of F_{CH4}. In the future, water table dynamics at Scotty Creek could be altered by increasing growing season evapotranspiration (Helbig *et al.*, 2016c), and/or changing snowmelt inputs (Houghton *et al.*, in preparation) and drainage patterns (Connon *et al.*, 2014). Interannual and long-term water table changes may then alter F_{CH4_LAND}; better projections of hydrological conditions in the future would therefore strengthen our ability to predict future F_{CH4_LAND} in the lowland boreal zone of North America (e.g., Lawrence *et al.*, 2015).

Wetland extent as control on spatial F_{CH4} variation

At Scotty Creek, F_{CH4_LAND} of the thawing boreal forest-wetland landscape increases with wetland extent (Fig. 3). Forests with permafrost are characterized by relatively dry, cold soils with a thick unsaturated zone. In contrast, the wetlands are permafrost-free, warmer, and have water tables that remain close to the moss surface due to differences in local topography between the forest and wetland surfaces (Fig. S2). Methane production is enhanced and oxidation is reduced in the warmer saturated wetland soils (e.g., Sundh *et al.*, 1994). In the permafrost-affected forest soils, aerobic soil conditions and the cooler T_{s_FOR} may result in smaller methanogen populations, unresponsive to soil temperature variations, thus suppressing CH_4 production (Yavitt *et al.*, 2006). Consequently, F_{CH4_LAND} increases with increasing wetland-to-forest ratio due to the characteristic differences in soil thermal and moisture conditions related to the absence of permafrost in wetlands and presence of permafrost in the forests (Baltzer *et al.*, 2014).

Previous chamber flux measurements at similar boreal peatlands corroborate the larger CH_4 emissions of permafrost-free wetlands compared to forested permafrost peat plateaus (Bubier *et al.*, 1995; Liblik *et al.*, 1997; Turetsky *et al.*, 2002). Forested permafrost peat plateaus have been identified as small net CH_4 sinks (> -0.1 g CH_4 m^{-2} yr^{-1}; Flessa *et al.*, 2008, Liblik *et al.*, 1997, Turetsky *et al.*, 2002, Bubier *et al.*, 2005) or small net CH_4 sources (< +20 mg CH_4 m^{-2} d^{-1}; Bubier *et al.*, 1995) with net CH_4 sink-source strengths only weakly depending on soil temperature (e.g., Bubier *et al.*, 2005). In accordance with our findings, Savage *et al.* (1997) report a chamber-based growing season ΣF_{CH4} estimate of 0.03±0.05 g CH_4 m^{-2} (May to September) for a forested permafrost peat plateau in northern Manitoba, Canada.

Integrated growing season landscape and wetland F_{CH4}

The growing season ΣF_{CH4_WET} of 13.0 g CH_4 m^{-2} (Fig. 5) compares well to the annual ΣF_{CH4} of 12.6 g CH_4 m^{-2} from a boreal minerotrophic fen in Finland (Rinne *et al.*, 2007), to the annual ΣF_{CH4} of 15.3 g CH_4 m^{-2} from a boreal poor fen in Sweden (Nilsson *et al.*, 2008), and to the growing season ΣF_{CH4} of 11 g CH_4 m^{-2} of a thawing sub-Arctic Swedish peatland complex (Johansson *et al.*, 2006), but is smaller than the growing season ΣF_{CH4} of 24.4 g CH_4 m^{-2} for a patterned boreal fen in Saskatchewan, Canada (Suyker *et al.*, 1996). In contrast, growing season ΣF_{CH4_WET} at Scotty Creek exceed the growing season ΣF_{CH4} of collapse-scar bogs in Alaska (see studies by Wickland *et al.*, 2006; Myers-Smith *et al.*, 2007; Euskirchen *et al.*, 2014; Tab. 3). The July and August ΣF_{CH4} of 6.2 g CH_4 m^{-2} reported by Liblik *et al.* (1997) for a collapse-scar bog in the southern Taiga Plains compares well to the 6.6 g CH_4 m^{-2} for July and August 2014 at the wetland at Scotty Creek. Similarly, the growing season ΣF_{CH4} of 11.4 g CH_4 m^{-2} (15 May - 15 September) reported by Bubier *et al.* (1995) for a collapse-scar bog in northern Manitoba, Canada, is of similar magnitude as the May to September ΣF_{CH4_WET} of 11.6 g CH_4 m^{-2} found in this study. Growing season ΣF_{CH4} for forested peatlands range between -0.1 g CH_4 m^{-2} and 1.1 g CH_4 m^{-2} (Tab. 3), suggesting that, generally, net CH_4 fluxes from these peatlands are negligible compared to treeless wetlands.

In this study, ΣF_{CH4_WET} and ΣF_{CH4_LAND} do not include winter ΣF_{CH4}. During winter, surface peat in the wetlands overlays unfrozen peat deposits while forest peat soils are frozen through the entire profile (Fig. S2). However, small but continuously positive F_{CH4} during long boreal winters have been shown to substantially (>10 %) contribute to annual ΣF_{CH4} of boreal wetlands and other high-latitude ecosystems (e.g., Rinne *et al.*, 2007; Jackowicz-Korczynski *et al.*, 2010; Christensen *et al.*, 2012; Zona *et al.*, 2016). For our study site, we expect forests with negligible growing season F_{CH4_FOR} also to be negligible winter CH_4 sinks-sources. Using average F_{CH4_WET} and F_{CH4_LAND} in November, March, and April (wetland [n = 233] and landscape tower [n = 1375]), winter ΣF_{CH4_WET} and ΣF_{CH4_LAND} (snow-cover period: November – April) are estimated to account for 3.3 g CH_4 m^{-2} (25 % of snow-free ΣF_{CH4_WET}) and 1.5 g CH_4 m^{-2} (23 % of snow-free ΣF_{CH4_LAND}), respectively. These winter estimates are derived with open-path CH_4 gas analyzers and need to be cautiously interpreted because large density effects (WPL term) and small "true" F_{CH4} may lead to large relative F_{CH4} uncertainties (Goulden *et al.*, 2006). A small bias accumulated over several months could lead to an under- or overestimation of winter ΣF_{CH4}. Additionally, ΣF_{CH4} derived from eddy covariance measurements may be underestimated by up to 20 %, as indicated by the widespread observation of surface energy balance non-closure at flux tower sites (Stoy *et al.*, 2013). We therefore assume that growing season ΣF_{CH4_WET} and ΣF_{CH4_LAND} for Scotty Creek represent conservative estimates of annual ΣF_{CH4_WET} and ΣF_{CH4_LAND}, mainly due to the significant but poorly constrained contribution of non-growing season fluxes.

Thaw-induced change in landscape F_{CH4}

Several studies have reported on seasonal CH_4 emissions from boreal peatlands (e.g. Moore *et al.*, 1994; Suyker *et al.*, 1996; Rinne *et al.*, 2007; Tab. 3), some provided up-scaled CH_4 budgets for boreal landscapes including peatlands (e.g., Liblik *et al.*, 1997; Bubier *et al.*, 2005; Flessa *et al.*, 2008), but few analyzed thaw-induced changes in landscape CH_4 emissions (e.g., Johansson *et al.* (2006) for a sub-Arctic treeless peatland complex). How changing landscape structure and composition in the North American permafrost zone perturbs boreal forest-wetland landscape ΣF_{CH4} has not been addressed yet. Here, we have quantified thaw impacts on F_{CH4_LAND} using a nested eddy covariance tower setup.

The thaw-induced conversion of non-CH_4 emitting forests to CH_4-emitting wetlands strengthens the growing season landscape net CH_4 emissions (ΣF_{CH4_LAND}) by 0.034±0.007 g CH_4 m^{-2} yr^{-1} at Scotty Creek (Fig. 6). As an integrated measure of ΣF_{CH4_LAND}, eddy covariance measurements, as used in this study, avoid uncertainties characteristic for the up-scaling of small-scale, chamber-based F_{CH4} measurements related to discontinuous temporal sampling and spatial under-sampling of CH_4 emission "hot spots" (e.g., Bubier *et al.*, 2005; Knohl *et al.*, 2008). The increasing CH_4 emissions in boreal forest-wetland landscapes can be supported by the large organic C amounts stored in forested peat plateaus (105±40 kg C m^{-2} for the 42 forested peat plateaus in Fig. 6; Treat *et al.*, 2016). Our conservative estimate of ΣF_{CH4_LAND} changes could be exceeded in the future with increasing annual air temperatures potentially extending the growing season length and thus the period with environmental conditions favorable for CH_4 production (e.g., warm T_{s_WET}; Moore *et al.*, 1998). Additionally, change rates of ΣF_{CH4_LAND} may be larger as estimated in this study if wetland expansion accelerates along with increasingly warmer air temperatures and increased landscape fragmentation (Baltzer *et al.*, 2014; Lara *et al.*, 2016).

In contrast, some models project a decrease in ΣF_{CH4} in the permafrost zone in response to climate warming and thawing permafrost (e.g., Lawrence *et al.*, 2015). For example, the Community Land Model (CLM) projects a decrease in high-latitude ΣF_{CH4} due to its predicted improved drainage conditions following permafrost thaw, and drier soils limiting CH_4 production (e.g., Koven *et al.*, 2011; Lawrence *et al.*, 2015). However, the current CLM, similar to other land surface schemes, does not account for thaw-induced land surface subsidence and thus may not adequately capture future wetland extents in lowland boreal forest-wetland landscapes (Gao *et al.*, 2013; Lee *et al.*, 2014).

Net radiative greenhouse gas forcing due to increasing landscape ΣF_{CH4}

Wetlands act as long-term net CO_2 sinks and CH_4 sources (Frolking *et al.*, 2011). During the first decades to centuries, emerging wetlands usually exert a positive net radiative greenhouse gas forcing (warming effect) due to the CH_4 warming effect exceeding the cooling effect of net CO_2 uptake. Over longer time-scales, the net radiative greenhouse gas forcing eventually becomes negative (cooling effect) because the CO_2 cooling effect exceeds the CH_4 warming effect, even with constant CO_2 sink and CH_4 source strengths (Frolking *et al.*, 2006). Calculating the global warming potential (GWP) using a fixed timeframe neglects this temporal evolution of net radiative greenhouse gas forcing from peatlands and, by definition, does not account for temporally varying net CO_2 sink- and CH_4 source-strengths (Neubauer & Megonigal, 2015). Here, the warming effects of a steadily increasing landscape CH_4 source likely exceed the cooling effects of a continuous peatland net CO_2 sink through the 21st century in the dynamic net radiative greenhouse gas forcing model (Fig. 6). The net CO_2 uptake is derived using two approaches: eddy covariance net CO_2 flux measurements and long-term C accumulation rates of similar peatland types in the permafrost zone (Treat *et al.*, 2016). At some peatlands affected by permafrost thaw, previously frozen, relatively labile organic C in forested peat plateaus may decompose rapidly upon thaw and may weaken the contemporary peatland net CO_2 sink in the future (O'Donnell *et al.*, 2011), further increasing the positive net radiative greenhouse gas forcing. However, the landscape NEE measurements at Scotty Creek still indicate a landscape net CO_2 sink, despite rapidly thawing permafrost (Fig. 6).

Landscape net CO_2 uptake may vary depending on the dominant peatland types in the region. At Scotty Creek, the annual eddy covariance landscape NEE of -71 g CO_2 m^{-2} compares well to the median long-term forested peat plateau net CO_2 uptake rate of 78 g CO_2 m^{-2} and to the median bog uptake rate of 88 g CO_2 m^{-2} (Treat *et al.*, 2016). In contrast, the annual CO_2 uptake derived from eddy covariance landscape NEE measurements was only half of the long-term fen net CO_2 uptake from similar landscapes (Fig. 6). At the same time, fens generally emit more CH_4 (Olefeldt *et al.*, 2013; Tab. 3). Channel fens at Scotty Creek, similar to collapse-scar bogs, expand with permafrost thaw (Quinton *et al.*, 2011), but are not captured by the landscape flux footprints (Helbig *et al.*, 2016c). Channel fen F_{CH4} studies could therefore help further constraining the thaw-induced net radiative greenhouse gas forcing.

To better predict wetland expansion in the permafrost zone, improved large-scale mapping of poorly drained, organic-rich lowland boreal forests (e.g., Thompson *et al.*, 2016) is required, as these landscapes are most sensitive to thaw-induced wetland expansion (Helbig *et al.*, 2016a; Lara *et al.*, 2016). The future trajectories of wetland expansion may also depend on increased atmospheric water inputs to sustain high water tables. The water demand could be satisfied by projected increases in water availability at high latitudes (Lawrence *et al.*, 2015).

Here, we show that the climate warming effect of thaw-induced ΣF_{CH4} increases in a boreal forest-wetland landscape likely exceeds the cooling effect of long-term net CO_2 uptake over the current century (i.e., a positive net radiative greenhouse gas forcing; Fig. 6). However, the thaw-induced wetland expansion in the southern Taiga Plains also induces regional climate cooling due to increases in albedo and decreases in sensible heat fluxes (Helbig *et al.*, 2016c). To quantify the total net radiative greenhouse gas forcing of wetland expansion in the sporadic permafrost zone and to compare it to its net radiative biophysical forcing, wetland expansion rates need to be up-scaled from local to regional scales.

In the southern Taiga Plains, current thaw-induced wetland expansion is already modifying how boreal peatlands in the sporadic permafrost zone interact with the global and regional climates. Process-based models aiming to predict such thaw impacts on climate thus need to account for various dynamic interactions between permafrost, local topography and regional hydrology, and F_{CH4}. Nested F_{CH4} measurements, such as presented in this study, offer an opportunity to evaluate the performance of such models to simulate and project changes in landscape CH_4 emissions against measured ecosystem and landscape F_{CH4}.

Acknowledgements

M. Helbig was funded through graduate student scholarships provided by the Fonds de recherche du Québec – Nature et technologies (FRQNT) and the German Academic Exchange Service (DAAD). Funding for this research was awarded to O. Sonnentag by the Canada Research Chairs, Canada Foundation for Innovation Leaders Opportunity Fund and Natural Sciences and Engineering Research Council Discovery Grant programs. C.T. acknowledges funding from the National Science Foundation (ARC-1304823). We are grateful for the support of the Liidlii Kue First Nation and Jean-Marie River First Nation for their support of the Scotty Creek Research Station. We thank Tim Moore for helpful comments on an earlier version of the manuscript and Matteo Detto (Smithsonian Tropical Research Institute) for valuable discussion on this manuscript. We also thank the two anonymous reviewers for their constructive comments.

References

Baltzer JL, Veness T, Chasmer LE, Sniderhan AE, Quinton WL (2014) Forests on thawing permafrost: fragmentation, edge effects, and net forest loss. *Global Change Biology*, **20**, 824–834.

Bellisario LM, Bubier JL, Moore TR (1999) Controls on CH_4 emissions from a northern peatland. *Global Biogeochemical Cycles*, **13**, 81–91.

Bousquet P, Ciais P, Miller JB et al. (2006) Contribution of anthropogenic and natural sources to atmospheric methane variability. *Nature*, **443**, 439–43.

Bridgham SD, Cadillo-Quiroz H, Keller JK, Zhuang Q (2013) Methane emissions from wetlands: biogeochemical, microbial, and modeling perspectives from local to global scales. *Global Change Biology*, **19**, 1325–1346.

Bubier JL, Moore TR, Bellisario L, Comer NT, Crill M (1995) Ecological controls on methane emissions from a northern peatland complex in the zone of discontinuous permafrost, Manitoba, Canada. *Global Biogeochemical Cycles*, **9**, 455–470.

Bubier J, Moore T, Savage K, Crill P (2005) A comparison of methane flux in a boreal landscape between a dry and a wet year. *Global Biogeochemical Cycles*, **19**, GB1023.

Camill P (1999) Patterns of boreal permafrost peatland vegetation across environmental gradients sensitive to climate warming. *Canadian Journal of Botany*, **77**, 721–733.

Camill P, Clark JS (1998) Climate change disequilibrium of boreal permafrost peatlands caused by local processes. *The American Naturalist*, **151**, 207–22.

Chanton JP, Glaser PH, Chasar LS et al. (2008) Radiocarbon evidence for the importance of surface vegetation on fermentation and methanogenesis in contrasting types of boreal peatlands. *Global Biogeochemical Cycles*, **22**, GB4022.

Chapin FS III, Woodwell GM, Randerson JT et al. (2006) Reconciling Carbon-cycle Concepts, Terminology, and Methods. *Ecosystems*, **9**, 1041–1050.

Chasmer L, Kljun N, Barr A, Black A, Hopkinson C, McCaughey H, Treitz P (2008) Influences of vegetation structure and elevation on CO_2 uptake in a mature jack pine forest in Saskatchewan, Canada. *Canadian Journal of Forest Research*, **38**, 2746–2761.

Chasmer L, Hopkinson C, Veness T, Quinton W, Baltzer J (2014) A decision-tree classification for low-lying complex land cover types within the zone of discontinuous permafrost. *Remote Sensing of Environment*, **143**, 73–84.

Christensen TR, Panikov NS, Oequist M, Svensson BH, Nykänen H, Martikainen PJ, Oskarsson H (2003) Factors controlling large scale variations in methane emissions from wetlands. *Geophysical Research Letters*, **30**, 10–13.

Christensen TR, Jackowicz-Korczyński M, Aurela M, Crill P, Heliasz M, Mastepanov M, Friborg T (2012) Monitoring the Multi-Year Carbon Balance of a Subarctic Palsa Mire with Micrometeorological Techniques. *AMBIO: A Journal of the Human Environment*, **41**, 207–217.

Connon RF, Quinton WL, Craig JR, Hayashi M (2014) Changing hydrologic connectivity due to permafrost thaw in the lower Liard River valley, NWT, Canada. *Hydrological Processes*,

28, 4163–4178.

Connon RF, Quinton WL, Craig JR, Hanisch J, Sonnentag O (2015) The hydrology of interconnected bog complexes in discontinuous permafrost terrains. *Hydrological Processes*, **29**, 3831–3847.

Desai AR, Xu K, Tian H et al. (2015) Landscape-level terrestrial methane flux observed from a very tall tower. *Agricultural and Forest Meteorology*, **201**, 61–75.

Dijk A Van, Moene AF, de Bruin HAR (2004) *The principles of surface flux physics: theory, practice and description of the ECPACK library, Internal Report 2004/1*. Wageningen, Netherlands, 99 pp.

Dlugokencky EJ, Bruhwiler L, White JWC et al. (2009) Observational constraints on recent increases in the atmospheric CH 4 burden. *Geophysical Research Letters*, **36**, L18803.

Dlugokencky EJ, Nisbet EG, Fisher R, Lowry D (2011) Global atmospheric methane: budget, changes and dangers. *Philosophical Transactions of the Royal Society*, **369**, 2058–2072.

Dunfield P, Knowles R, Dumont R, Moore TR (1993) Methane production and consumption in temperate and subarctic peat soils: Response to temperature and pH. *Soil Biology and Biochemistry*, **25**, 321–326.

Dunn AL, Barford CC, Wofsy SC, Goulden ML, Daube BC (2007) A long-term record of carbon exchange in a boreal black spruce forest: means, responses to interannual variability, and decadal trends. *Global Change Biology*, **13**, 577–590.

Euskirchen ES, Edgar CW, Turetsky MR, Waldrop MP, Harden JW (2014) Differential response of carbon fluxes to climate in three peatland ecosystems that vary in the presence and stability of permafrost. *Journal of Geophysical Research: Biogeosciences*, **119**, 1576–1595.

Flessa H, Rodionov A, Guggenberger G et al. (2008) Landscape controls of CH_4 fluxes in a catchment of the forest tundra ecotone in northern Siberia. *Global Change Biology*, **14**, 2040–2056.

Frolking S, Roulet N, Fuglestvedt J (2006) How northern peatlands influence the Earth's radiative budget: Sustained methane emission versus sustained carbon sequestration. *Journal of Geophysical Research*, **111**, G01008.

Frolking S, Talbot J, Jones MC, Treat CC, Kauffman JB, Tuittila E-S, Roulet NT (2011) Peatlands in the Earth's 21st century climate system. *Environmental Reviews*, **19**, 371–396.

Gao X, Adam Schlosser C, Sokolov A, Anthony KW, Zhuang Q, Kicklighter D (2013) Permafrost degradation and methane: low risk of biogeochemical climate-warming feedback. *Environmental Research Letters*, **8**, 035014.

Garon-Labrecque M-E, Léveillé-Bourret É, Higgins K, Sonnentag O (2015) Additions to the Boreal Flora of the Northwest Territories with a Preliminary Vascular Flora of Scotty Creek. *Canadian Field-Naturalist*, **129**, 349–367.

Goulden ML, Winston GC, McMillan AMS, Litvak ME, Read EL, Rocha A V., Rob Elliot J (2006) An eddy covariance mesonet to measure the effect of forest age on land-atmosphere exchange. *Global Change Biology*, **12**, 2146–2162.

Hanis KL, Tenuta M, Amiro BD, Papakyriakou TN (2013) Seasonal dynamics of methane emissions from a subarctic fen in the Hudson Bay Lowlands. *Biogeosciences*, **10**, 4465–

4479.

Hartley IP, Hill TC, Wade TJ et al. (2015) Quantifying landscape-level methane fluxes in subarctic Finland using a multiscale approach. *Global Change Biology*, **21**, 3712–3725.

Helbig M, Pappas C, Sonnentag O (2016a) Permafrost thaw and wildfire: equally important drivers of boreal tree cover changes in the Taiga Plains, Canada. *Geophysical Research Letters*, **43**, 1598-1606.

Helbig M, Wischnewski K, Gosselin GH et al. (2016b) Addressing a systematic bias in carbon dioxide flux measurements with the EC150 and the IRGASON open-path gas analyzers. *Agricultural and Forest Meteorology*, **228**, 349–359.

Helbig M, Wischnewski K, Kljun N, Chasmer L, Quinton WL, Detto M, Sonnentag O (2016c) Regional atmospheric cooling and wetting effect of permafrost thaw-induced boreal forest loss. *Global Change Biology*. doi:10.1111/gcb.13348.

Hommeltenberg J, Mauder M, Drösler M, Heidbach K, Werle P, Peter H (2014) Ecosystem scale methane fluxes in a natural temperate bog-pine forest in southern Germany. *Agricultural and Forest Meteorology*, **198-199**, 273–284.

Iwata H, Harazono Y, Ueyama M et al. (2015) Methane exchange in a poorly-drained black spruce forest over permafrost observed using the eddy covariance technique. *Agricultural and Forest Meteorology*, **214-215**, 157–168.

Jackowicz-Korczynski M, Christensen TR, Backstrand K, Crill P, Friborg T, Mastepanov M, Strom L (2010) Annual cycle of methane emission from a subarctic peatland. *Journal of Geophysical Research*, **115**, G02009.

Johansson T, Malmer N, Crill PM, Friborg T, Akerman JH, Mastepanov M, Christensen TR (2006) Decadal vegetation changes in a northern peatland, greenhouse gas fluxes and net radiative forcing. *Global Change Biology*, **12**, 2352–2369.

Johnston CE, Ewing S a, Harden JW et al. (2014) Effect of permafrost thaw on CO_2 and CH_4 exchange in a western Alaska peatland chronosequence. *Environmental Research Letters*, **9**, 085004.

Joos F, Roth R, Fuglestvedt JS et al. (2013) Carbon dioxide and climate impulse response functions for the computation of greenhouse gas metrics: A multi-model analysis. *Atmospheric Chemistry and Physics*, **13**, 2793–2825.

Kettunen A, Kaitala V, Lehtinen A, Lohila A, Alm J, Silvola J, Martikainen PJ (1999) Methane production and oxidation potentials in relation to water table fluctuations in two boreal mires. *Soil Biology and Biochemistry*, **31**, 1741–1749.

Kirschke S, Bousquet P, Ciais P et al. (2013) Three decades of global methane sources and sinks. *Nature Geoscience*, **6**, 813–823.

Klapstein SJ, Turetsky MR, McGuire AD et al. (2014) Controls on methane released through ebullition in peatlands affected by permafrost degradation. *Journal of Geophysical Research: Biogeosciences*, **119**, 418–431.

Kljun N, Calanca P, Rotach MW, Schmid HP (2015) A simple two-dimensional parameterisation for Flux Footprint Predictions (FFP). *Geoscientific Model Development*, **8**, 3695–3713.

Knohl A, Søe ARB, Kutsch WL, Göckede M, Buchmann N (2008) Representative estimates of soil and ecosystem respiration in an old beech forest. *Plant and Soil*, **302**, 189–202.

Koven CD, Ringeval B, Friedlingstein P et al. (2011) Permafrost carbon-climate feedbacks accelerate global warming. *Proceedings of the National Academy*, **108**, 14769–14774.

Lara MJ, Genet H, McGuire AD et al. (2016) Thermokarst rates intensify due to climate change and forest fragmentation in an Alaskan boreal forest lowland. *Global Change Biology*, **22**, 816–829.

Lasslop G, Reichstein M, Kattge J, Papale D (2008) Influences of observation errors in eddy flux data on inverse model parameter estimation. *Biogeosciences*, **5**, 1311–1324.

Lawrence DM, Koven CD, Swenson SC, Riley WJ, Slater AG (2015) Permafrost thaw and resulting soil moisture changes regulate projected high-latitude CO_2 and CH_4 emissions. *Environmental Research Letters*, **10**, 094011.

Lee H, Swenson SC, Slater AG, Lawrence DM (2014) Effects of excess ground ice on projections of permafrost in a warming climate. *Environmental Research Letters*, **9**, 124006.

Legendre P, Legendre L (2012) *Numerical Ecology*, 3rd edn. Elsevier B.V., Amsterdam, The Netherlands, 990 pp.

Liblik L, Moore TR, Bubier JL, Robinson SD (1997) Methane emissions from wetland in the zone of discontinuous permafrost: Fort Simpson, Northwest Territories, Canada. *Global Biogeochemical Cycles*, **11**, 485–494.

Loisel J, Yu Z, Beilman DW et al. (2014) A database and synthesis of northern peatland soil properties and Holocene carbon and nitrogen accumulation. *The Holocene*, **24**, 1028–1042.

Mahecha MD, Reichstein M, Lange H et al. (2007) Characterizing ecosystem-atmosphere interactions from short to interannual time scales. *Biogeosciences*, **4**, 743–758.

Mauder M, Foken T (2011) *Documentation and Instruction Manual of the Eddy-Covariance Software Package TK3*. Bayreuth, Germany, 1-60 pp.

McDermitt D, Burba G, Xu L et al. (2010) A new low-power, open-path instrument for measuring methane flux by eddy covariance. *Applied Physics B*, **102**, 391–405.

Melton JR, Wania R, Hodson EL et al. (2013) Present state of global wetland extent and wetland methane modelling: conclusions from a model inter-comparison project (WETCHIMP). *Biogeosciences*, **10**, 753–788.

Moffat AM, Papale D, Reichstein M et al. (2007) Comprehensive comparison of gap-filling techniques for eddy covariance net carbon fluxes. *Agricultural and Forest Meteorology*, **147**, 209–232.

Moncrieff JB, Malhi Y, Leuning R (1996) The propagation of errors in long-term measurements of land-atmosphere fluxes of carbon and water. *Global Change Biology*, **2**, 231–240.

Moncrieff JB, Massheder JM, de Bruin H et al. (1997) A system to measure surface fluxes of momentum, sensible heat, water vapour and carbon dioxide. *Journal of Hydrology*, **188-189**, 589–611.

Moncrieff J, Clement R, Finnigan J, Meyers T (2004) Averaging, detrending, and filtering of eddy covariance time series. In: *Handbook of Micrometeorology* (eds Lee X, Massman WJ, Law B), pp. 7–31. Springer Netherlands, Amsterdam, The Netherlands.

Moore TR (2003) Dissolved organic carbon in a northern boreal landscape. *Global Biogeochemical Cycles*, **17**, 1109.

Moore TR, Heyes A, Roulet NT (1994) Methane emissions from wetlands, southern Hudson Bay Lowland. *Journal of Geophysical Research-Atmospheres*, **99**, 1455–1467.

Moore TR, Roulet NT, Waddington JM (1998) Uncertainty in predicting the effect of climatic change on the carbon cycling of canadian peatlands. *Climatic Change*, **40**, 229–245.

Moore TR, Young A, Bubier JL, Humphreys ER, Lafleur PM, Roulet NT (2011) A multi-year record of methane flux at the Mer Bleue Bog, southern Canada. *Ecosystems*, **14**, 646–657.

Myers-Smith IH, McGuire AD, Harden JW, Chapin FS III (2007) Influence of disturbance on carbon exchange in a permafrost collapse and adjacent burned forest. *Journal of Geophysical Research*, **112**, G04017.

Myhre G, Shindell D, Bréon F-M et al. (2013) Anthropogenic & Natural Radiative Forcing. In: *Climate Change 2013: The Physical Science Basis. Contribution of Working Group I to the Fifth Assessment Report of the Intergovernmental Panel on Climate Change* (eds Stocker TF, Qin D, Plattner G-K, Tignor M, Allen SK, Boschung J, Nauels A, Xia Y, Bex V, Midgley PM), pp. 659–740. Cambridge University Press, Cambridge, United Kingdom and New York, NY, USA.

Neubauer SC (2014) On the challenges of modeling the net radiative forcing of wetlands: reconsidering Mitsch et al. 2013. *Landscape Ecology*, **29**, 571–577.

Neubauer SC, Megonigal JP (2015) Moving beyond Global Warming Potentials to quantify the climatic role of ecosystems. *Ecosystems*, **18**, 1000–1013.

Nilsson M, Sagerfors J, Buffam I et al. (2008) Contemporary carbon accumulation in a boreal oligotrophic minerogenic mire - A significant sink after accounting for all C-fluxes. *Global Change Biology*, **14**, 2317–2332.

Nisbet EG, Dlugokencky EJ, Bousquet P (2014) Methane on the rise - again. *Science*, **343**, 493–495.

O'Donnell JA, Harden JW, McGuire AD, Kanevskiy MZ, Jorgenson MT, Xu X (2011) The effect of fire and permafrost interactions on soil carbon accumulation in an upland black spruce ecosystem of interior Alaska: implications for post-thaw carbon loss. *Global Change Biology*, **17**, 1461–1474.

Olefeldt D, Roulet NT, Bergeron O, Crill P, Bäckstrand K, Christensen TR (2012) Net carbon accumulation of a high-latitude permafrost palsa mire similar to permafrost-free peatlands. *Geophysical Research Letters*, **39**, L03501.

Olefeldt D, Turetsky MR, Crill PM, McGuire AD (2013) Environmental and physical controls on northern terrestrial methane emissions across permafrost zones. *Global Change Biology*, **19**, 589–603.

Papale D, Reichstein M, Aubinet M et al. (2006) Towards a standardized processing of Net Ecosystem Exchange measured with eddy covariance technique: algorithms and uncertainty estimation. *Biogeosciences*, **3**, 571–583.

Prater JL, Chanton JP, Whiting GJ (2007) Variation in methane production pathways associated with permafrost decomposition in collapse scar bogs of Alberta, Canada. *Global*

Biogeochemical Cycles, **21**, GB4004.

Quinton WL, Hayashi M, Chasmer LE (2011) Permafrost-thaw-induced land-cover change in the Canadian subarctic: implications for water resources. *Hydrological Processes*, **25**, 152–158.

Rask H, Schoenau J, Anderson D (2002) Factors influencing methane flux from a boreal forest wetland in Saskatchewan, Canada. *Soil Biology and Biochemistry*, **34**, 435–443.

Reichstein M, Falge E, Baldocchi D et al. (2005) On the separation of net ecosystem exchange into assimilation and ecosystem respiration: review and improved algorithm. *Global Change Biology*, **11**, 1424–1439.

Rinne J, Riutta T, Pihlatie M et al. (2007) Annual cycle of methane emission from a boreal fen measured by the eddy covariance technique. *Tellus, Series B: Chemical and Physical Meteorology*, **59**, 449–457.

Roulet NT, Lafleur PM, Richard PJH, Moore TR, Humphreys ER, Bubier J (2007) Contemporary carbon balance and late Holocene carbon accumulation in a northern peatland. *Global Change Biology*, **13**, 397–411.

Savage K, Moore TR, Crill PM (1997) Methane and carbon dioxide exchanges between the atmosphere and northern boreal forest soils. *Journal of Geophysical Research*, **102**, 29,279–29,288.

Schoellhamer DH (2001) Singular spectrum analysis for time series with missing data. *Geophysical Research Letters*, **28**, 3187–3190.

Schuur EAG, McGuire AD, Schädel C et al. (2015) Climate change and the permafrost carbon feedback. *Nature*, **520**, 171–179.

Shannon RD, White JR (1994) A three-year study of controls on methane emissions from two Michigan peatlands. *Biogeochemistry*, **27**, 35–60.

Sonnentag O, Van Der Kamp G, Barr AG, Chen JM (2010) On the relationship between water table depth and water vapor and carbon dioxide fluxes in a minerotrophic fen. *Global Change Biology*, **16**, 1762–1776.

Stoy PC, Mauder M, Foken T et al. (2013) A data-driven analysis of energy balance closure across FLUXNET research sites: The role of landscape scale heterogeneity. *Agricultural and Forest Meteorology*, **171-172**, 137–152.

Sundh I, Nilsson M, Granberg G, Svensson BH (1994) Depth distribution of microbial production and oxidation of methane in northern boreal peatlands. *Microbial Ecology*, **27**, 253–265.

Suyker AE, Verma SB, Clement RJ, Billesbach DP (1996) Methane flux in a boreal fen: Season-long measurement by eddy correlation. *Journal of Geophysical Research*, **101**, 28,637–28,647.

Tarnocai C, Canadell JG, Schuur EAG, Kuhry P, Mazhitova G, Zimov S (2009) Soil organic carbon pools in the northern circumpolar permafrost region. *Global Biogeochemical Cycles*, **23**, GB2023.

Thompson DK, Simpson BN, Beaudoin A (2016) Using forest structure to predict the distribution of treed boreal peatlands in Canada. *Forest Ecology and Management*, **372**, 19–27.

Treat CC, Bubier JL, Varner RK, Crill PM (2007) Timescale dependence of environmental and plant-mediated controls of CH_4 flux in a temperate fen. *Journal of Geophysical Research: Biogeosciences*, **112**, G01014.

Treat CC, Wollheim WM, Varner RK, Grandy a S, Talbot J, Frolking S (2014) Temperature and peat type control CO_2 and CH_4 production in Alaskan permafrost peats. *Global Change Biology*, **20**, 2674–2686.

Treat CC, Jones MC, Camill P et al. (2016) Effects of permafrost aggradation on peat properties as determined from a pan-Arctic synthesis of plant macrofossils. *Journal of Geophysical Research: Biogeosciences*, **121**, 78–94.

Turetsky MR, Wieder RK, Vitt DH (2002) Boreal peatland C fluxes under varying permafrost regimes. *Soil Biology and Biochemistry*, **34**, 907–912.

Vickers D, Mahrt L (1997) Quality Control and Flux Sampling Problems for Tower and Aircraft Data. *Journal of Atmospheric and Oceanic Technology*, **14**, 512–526.

Webb EK, Pearman GI, Leuning R (1980) Correction of flux measurements for density effects due to heat and water vapour transfer. *Quarterly Journal of the Royal Meteorological Society*, **106**, 85–100.

Wickland KP, Striegl RG, Neff JC, Sachs T (2006) Effects of permafrost melting on CO_2 and CH_4 exchange of a poorly drained black spruce lowland. *Journal of Geophysical Research*, **111**, G02011.

Yavitt JB, Basiliko N, Turetsky MR, Hay AG (2006) Methanogenesis and Methanogen Diversity in Three Peatland Types of the Discontinuous Permafrost Zone, Boreal Western Continental Canada. *Geomicrobiology Journal*, **23**, 641–651.

Zona D, Gioli B, Commane R et al. (2016) Cold season emissions dominate the Arctic tundra methane budget. *Proceedings of the National Academy of Science*, **113**, 40–45.

Tab. 1: Linear regression statistics and 95 % confidence intervals (CI) of wetland against landscape methane fluxes for different classes of wetland footprint (FP) contributions.

Tab. 2: Best-fit Q_{10}-model parameters and corresponding 95 % confidence intervals (CI) and regression statistics of measured against modeled methane fluxes. Model fits were conducted for classes of varying forest contribution to flux footprints (FP).

Tab. 3: Cumulative methane fluxes (ΣF_{CH4}) derived from growing season F_{CH4} studies for different types of boreal peatlands with or without permafrost (PF). Studies refer to varying lengths of measurement periods and, for comparison, ΣF_{CH4} are normalized for periods of 120 days (i.e., mean daily F_{CH4} x 120 days). Studies are either based on eddy covariance (EC) or chamber (CH) flux measurements.

Fig. 1: Decomposition of net CH_4 flux measurements (F_{CH4}; nmol m^{-2} s^{-1}) into seasonal (F_{CH4_sf}; > seven days) and sub-weekly signals (F_{CH4_hf}; two hours – seven days) for the (a & b) landscape and the (c & d) wetland tower for the 2014 and 2015 growing seasons.

Fig. 2: Linear regression slopes between wetland contributions to landscape flux footprints and landscape methane fluxes (F_{CH4_LAND}), and mean differences in soil temperatures at a depth of 32 cm in the wetland (T_{s_WET}) and the forest (T_{s_FOR}) for three-day windows. The dashed line shows best linear fit and the shaded area the 95 % confidence interval of the regression.

Fig. 3: (a) Wetland (F_{CH4_WET}) and landscape methane fluxes (F_{CH4_LAND}) and linear regressions (see Tab. 1) for increasing classes of wetland contribution to landscape flux footprints. Dots are colored according to wetland contribution to landscape flux footprints and best-fit regression lines are colored according to the median of the respective wetland contribution class. (b) Best-fit Q_{10}-models (see Tab. 2) for classes of varying forest contributions to (wetland and landscape) flux footprints (solid lines) and measured methane fluxes (F_{CH4}, grey dots) against soil temperature at the wetland (T_{s_WET}). The dashed line indicates the estimated Q_{10}-model for forest-only contributions (i.e., F_{CH4_FOR}).

Fig. 4: Monthly cumulative growing season methane fluxes (ΣF_{CH4}) at (a) the landscape tower (2013-2016) and (b) the wetland tower (2014-2016) and (c) growing season dynamics of wetland water table depth (WTD) and soil temperature at 32 cm (T_{s_WET}) for three years. WTD and T_{s_WET} measurements started in 2014.

Fig. 5: Cumulative growing season CH_4 fluxes (ΣF_{CH4}) at the landscape tower and the wetland tower. Growing season fluxes in 2014 and 2015 were combined to derive a full growing season budget. Shaded areas indicate ΣF_{CH4} uncertainties due to the selection of the friction velocity threshold and due to random observation and gap-filling errors.

Fig. 6: Net radiative greenhouse gas forcing of the thaw-induced (i.e., wetland expansion) increase in growing season landscape CH_4 fluxes (ΣF_{CH4_LAND}) referenced to the year 1977. The solid red line represents the scenario with no net CO_2 uptake. Dashed lines show net radiative forcing for varying levels of annual net CO_2 uptake (ΣF_{CO2}) and for annual net ecosystem CO_2 exchange (NEE) measured at the landscape tower (unpublished data): negative signs indicate a net CO_2 uptake. The shaded area defines the range of net radiative forcing for long-term ΣF_{CO2} of similar peatlands including the uncertainty in the wetland expansion rate estimate. Long-term ΣF_{CO2} is based on the 90 % confidence interval (CI) of long-term apparent carbon accumulation rates (for “forested peat plateaus”, ”bogs”, ”fens”; Treat et al., 2016). Dotted lines indicate the net radiative forcing for median net CO_2 uptake rates for different peatland types. 1 fW = 10^{-15} Watts.

Tab. 1: Linear regression statistics and 95 % confidence intervals (CI) of wetland against landscape methane fluxes for different classes of wetland footprint (FP) contributions.

wetland FP contribution	slope	CI	intercept	CI	r^2	*n*
10 % - <30 %	0.34	0.27-0.43	0.1	-4.5-4.3	0.23	257
30 % - <50 %	0.43	0.36-0.5	4.4	1.1-7.4	0.28	505
50 % - <70 %	0.61	0.54-0.68	1.2	-1.4-3.6	0.53	330
70 % - <90 %	0.74	0.69-0.79	-1.8	-4.3-0.5	0.62	580

Tab. 2: Best-fit Q_{10}-model parameters and corresponding 95 % confidence intervals (CI) and regression statistics of measured against modeled methane fluxes. Model fits were conducted for classes of varying forest contribution to flux footprints (FP).

Forest FP contribution	F_{CH4_base}	CI	Q_{10}	CI	r^2	*n*
0% - <10 %	56.1	55.4 - 56.9	2.5	2.5 - 2.6	0.69	2152
10 % - <30 %	39.3	38.6 - 40.0	2.6	2.5 - 2.8	0.59	1746
30 % - <50 %	28.1	27.9 - 29.1	3.0	2.8 - 3.3	0.48	1048
50 % - <70 %	23.0	22.3 - 23.8	3.1	2.8 - 3.4	0.36	1788
70 % - <90 %	19.7	17.9 - 21.2	3.7	2.8 - 5.1	0.35	324

Tab. 3: Cumulative methane fluxes (ΣF_{CH4}) derived from growing season F_{CH4} studies for different types of boreal peatlands with or without permafrost (PF). Studies refer to varying lengths of measurement periods and, for comparison, ΣF_{CH4} are normalized for periods of 120 days (i.e., mean daily F_{CH4} x 120 days). Studies are either based on eddy covariance (EC) or chamber (CH) flux measurements.

Ecosystem type	PF	ΣF_{CH4} [study period] g CH_4 m^{-2}	Study period	ΣF_{CH4} [120 days] g CH_4 m^{-2}	Method	Reference
collapse-scar bog	no	5.0	21 Apr - 21 Sep	3.9	EC	Euskirchen *et al.*, 2014
collapse-scar bog	no	6.2	01 Jul - 31 Aug	12.5	CH	Liblik et al., 1997
collapse-scar bog	no	2.0	15 Jun - 19 Sep	2.4	CH	Myers-Smith *et al.*, 2007
collapse-scar bog	no	2.0	16 May - 20 Sep	1.6	CH	Wickland *et al.*, 2006
collapse-scar bog	no	11.8	15 May - 15 Sep	10.4	CH	Bubier et al., 1995
collapse-scar bog	no	13.0	01 Apr - 31 Oct	7.3	EC	this study
forested peat plateau	yes	0.0	01 Jul - 31 Aug	-0.1	CH	Liblik et al., 1997
forested peat plateau	yes	1.1	16 May - 20 Sep	0.8	CH	Wickland et al., 2006
forested peat plateau	yes	0.0	15 May - 15 Sep	0.0	CH	Savage et al., 1997
black spruce forest	yes	0.4	14 May - 07 Oct	0.3	EC	Iwata *et al.*, 2015
treed bog	yes	0.4	10 Jun - 15 Oct	0.4	CH	Moore et al., 1994
treeless bog plateau	yes	-0.1	01 Aug - 31 Nov	-0.1	CH	Flessa *et al.*, 2008
palsa fen	yes	6.9	30 May - 16 Nov	4.9	EC	Hanis *et al.*, 2013
minerotrophic fen	no	24.4	19 May - 04 Oct	21.0	EC	Suyker *et al.*, 1996
minerotrophic fen	no	11.4	29 Apr – 30 Nov	6.3	EC	Rinne *et al.*, 2007
collapse-scar fen	no	8.7	15 May - 15 Sep	8.4	CH	Bubier et al., 1995
palsa mire	yes/no	23.0	18 Apr - 22 Oct	14.8	EC	Jackowicz-Korczynski *et al.*, 2010
boreal forest-wetland	yes/no	6.7	01 Apr - 31 Oct	3.8	EC	this study

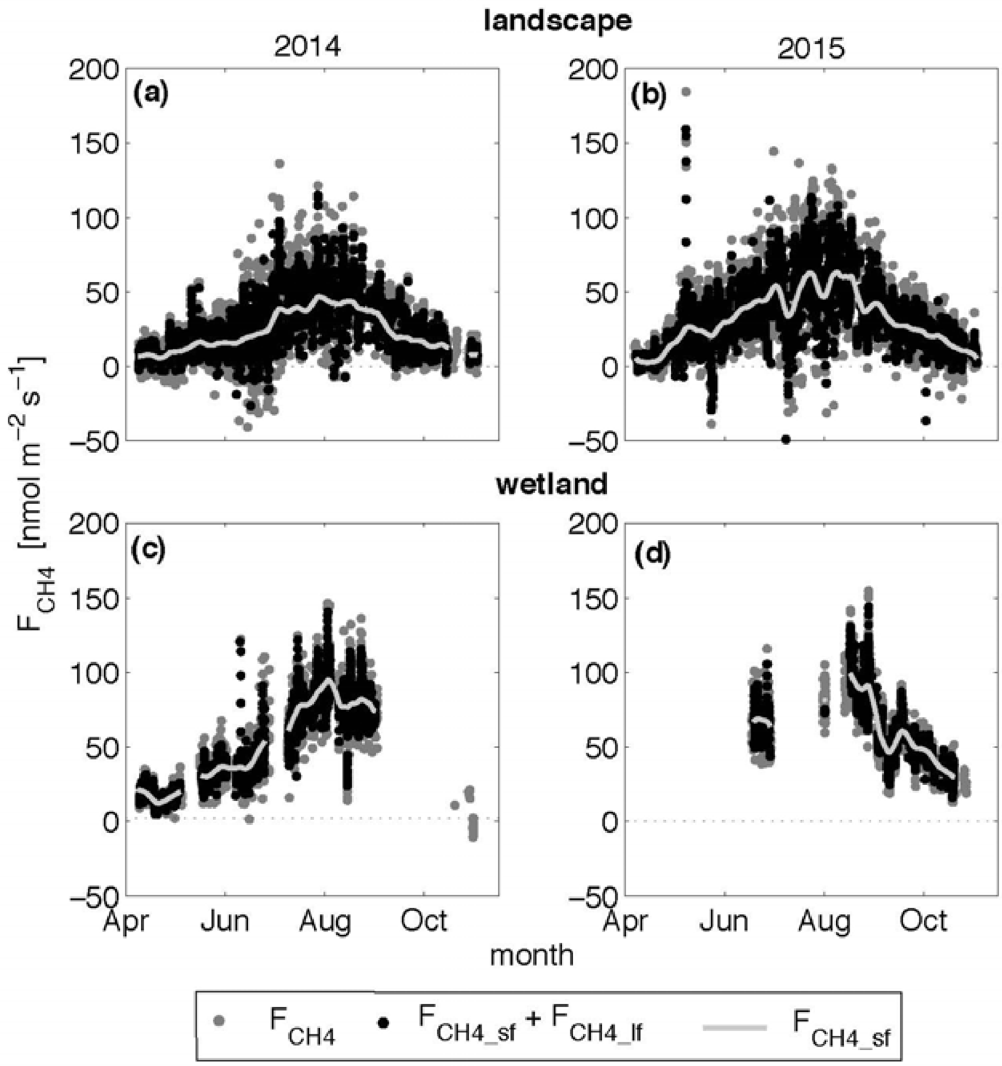
landscape
2014
2015
(a)
(b)
wetland
(c)
(d)
F_{CH4} [nmol m^{-2} s^{-1}]
200
150
100
50
0
−50
Apr
Jun
Aug
Oct
month
F_{CH4}
$F_{CH4\_sf} + F_{CH4\_lf}$
F_{CH4_sf}

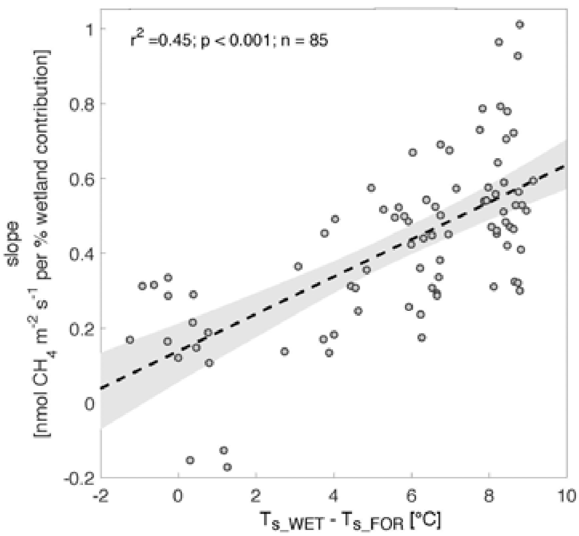
r^2 =0.45; p < 0.001; n = 85
slope
[nmol CH$_4$ m^{-2} s^{-1} per % wetland contribution]
T$_{s_WET}$ - T$_{s_FOR}$ [°C]

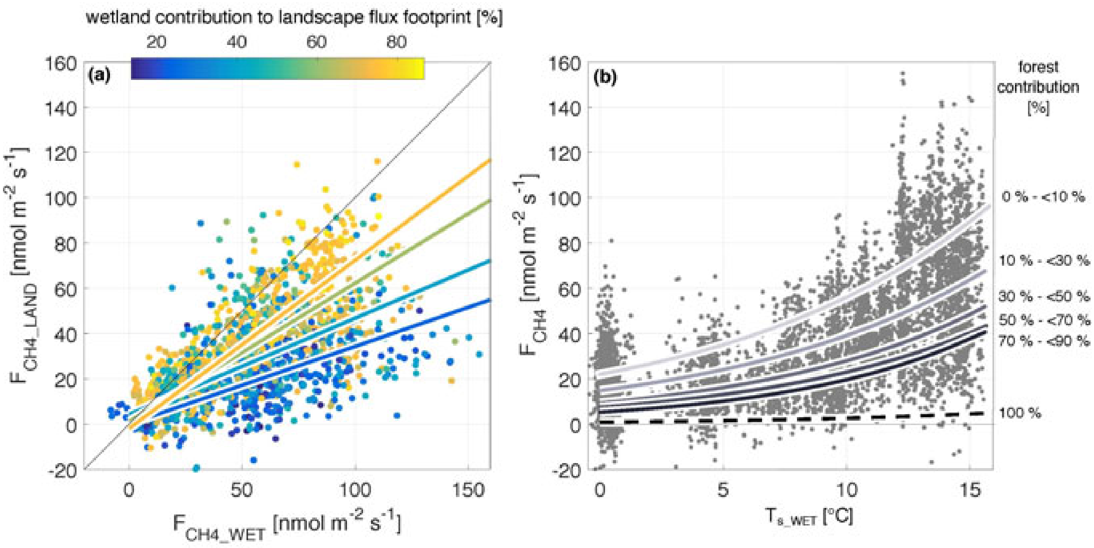
wetland contribution to landscape flux footprint [%]
20
40
60
80
(a)
F$_{CH4_LAND}$ [nmol m^{-2} s^{-1}]
F$_{CH4_WET}$ [nmol m^{-2} s^{-1}]
(b)
forest contribution [%]
0 % - <10 %
10 % - <30 %
30 % - <50 %
50 % - <70 %
70 % - <90 %
100 %
F$_{CH4}$ [nmol m^{-2} s^{-1}]
T$_{s_WET}$ [°C]

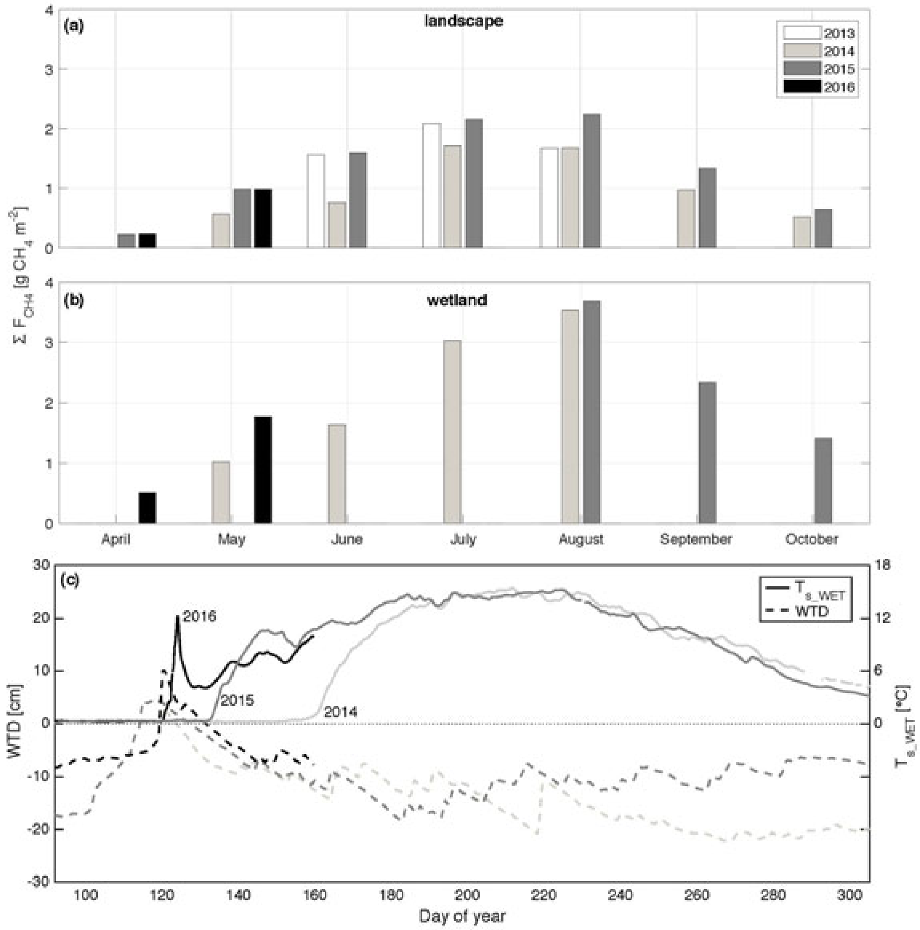
(a)
landscape
2013
2014
2015
2016
Σ F_{CH4} [g CH_4 m^{-2}]
(b)
wetland
April
May
June
July
August
September
October
(c)
T_{s_WET}
WTD
2016
2015
2014
WTD [cm]
T_{s_WET} [°C]
Day of year

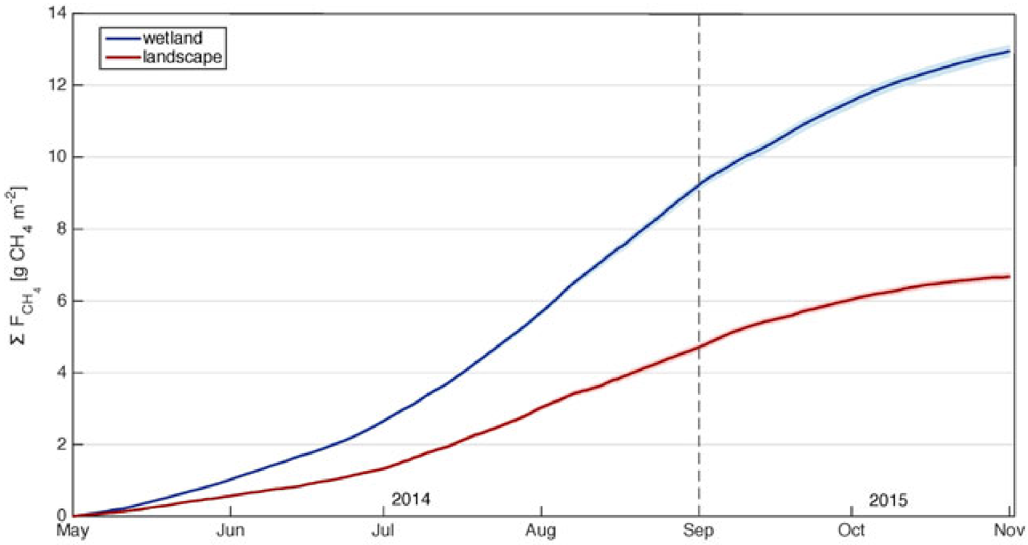
wetland
landscape
Σ F_{CH_4} [g CH_4 m^{-2}]
0
2
4
6
8
10
12
14
May
Jun
Jul
Aug
Sep
Oct
Nov
2014
2015

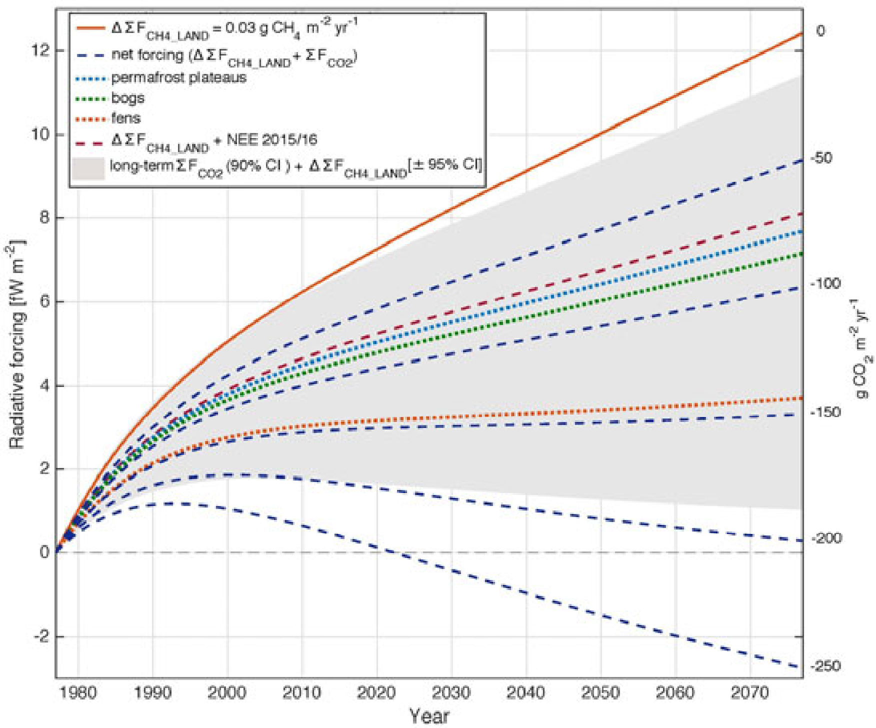
$\Delta\Sigma F_{CH4\_LAND}$ = 0.03 g CH_4 m^{-2} yr^{-1}
net forcing ($\Delta\Sigma F_{CH4\_LAND}$ + ΣF_{CO2})
permafrost plateaus
bogs
fens
$\Delta\Sigma F_{CH4\_LAND}$ + NEE 2015/16
long-term ΣF_{CO2} (90% CI) + $\Delta\Sigma F_{CH4\_LAND}$[± 95% CI]
Radiative forcing [fW m^{-2}]
g CO_2 m^{-2} yr^{-1}
Year
-2
0
2
4
6
8
10
12
0
-50
-100
-150
-200
-250
1980
1990
2000
2010
2020
2030
2040
2050
2060
2070